EUROPEAN ORGANIZATION FOR NUCLEAR RESEARCH

CERN-EP/88-102
23 August 1988

Direct photon production in $\bar{p}p$ collisions at $\sqrt{s} = 630$ GeV

The UA2 Collaboration

Bern[1] , *CERN*[2] , *Copenhagen(NBI)*[3] , *Heidelberg*[4]
Orsay(LAL)[5] , *Pavia*[6] , *Perugia*[7] , *Pisa*[8] , *Saclay(CEN)*[9]

R. Ansari[5], P. Bagnaia[2], M. Banner[9], R. Battiston[7], K. Bernlöhr[4]
C. Booth[2], K. Borer[1], M. Borghini[2], G. Carboni[8], V. Cavasinni[8]
P. Cenci[2,a], J.-C. Chollet[5], A.G. Clark[2,b], C. Conta[6], C. Corona[8]
F. Costantini[8], P. Darriulat[2], B. De Lotto[5,6], T. Del Prete[8], L. DiLella[2]
J. Dines Hansen[3], K. Einsweiler[2], L. Fayard[5], R. Ferrari[6], M. Fraternali[6]
D. Froidevaux[5], J.-M. Gaillard[5], O. Gildemeister[2], V.G. Goggi[6,2]
C. Gössling[2], B. Hahn[1], H. Hänni[2,c], J.R. Hansen[2,3], P. Hansen[3]
K. Hara[1], N. Harnew[2], H. Hugentobler[1], E. Iacopini[8]
L. Iconomidou-Fayard[5], K. Jakobs[4], P. Jenni[2], E.E. Kluge[4]
O. Kofoed-Hansen[3], S. Lami[8], E. Lançon[9], P.Lariccia[8,d], M. Livan[6]
S. Loucatos[9], B. Madsen[3], B. Mansoulié[9], G.C. Mantovani[7], L. Mapelli[2,e]
K. Meier[2], B. Merkel[5], R. Møllerud[3], M. Moniez[5], R. Moning[1]
M. Morganti[8,f], C. Onions[2], T. Pal[2], M.A. Parker[2], G. Parrour[5,2]
F. Pastore[6], M. Pepe[7,g], C. Petridou[2], H. Plothow-Besch[4]
M. Polverel[9], L. Rasmussen[2], J.-P. Repellin[5], A. Roussarie[9]
V. Ruhlmann[9], G. Sauvage[5], J. Schacher[1], S. Stapnes[2], F. Stocker[1,h]
M. Swartz[2,i], J. Teiger[9], W.Y. Tsang[2,j], M. Valdata-Nappi[8], V. Vercesi[6,2]
A.R. Weidberg[2], M. Wunsch[4] and H. Zaccone[9]

(subm. to Zeitschrift für Physik C)

Abstract

A measurement of the direct production of photons with high transverse momentum from $\bar{p}p$ collisions at $\sqrt{s} = 630$ GeV is presented. The structure of events containing a high transverse momentum photon is studied. The results support predictions from QCD theory.

[1]Laboratorium für Hochenergiephysik, Universität Bern, Sidlerstrasse 5, CH-3012 Bern, Switzerland

[2]CERN, CH-1211 Genève 23, Switzerland

[3]Niels Bohr Institute, Blegdamsvej 17, DK-2100 Copenhagen, Denmark

[4]Institut für Hochenergiephysik, Universität Heidelberg, Schröderstrasse 90, D-6900 Heidelberg, Germany

[5]LAL, Université de Paris-Sud, F-91405 Orsay Cedex, France

[6]Università di Pavia and INFN, Sezione di Pavia, Via Bassi 6, I-27100 Pavia, Italy

[7]Gruppo INFN del dipartimento di Fisica dell'Università di Perugia, I-106100 Perugia, Italy

[8]Università di Pisa and INFN, Via Livornese, S. Piero a Grado, I-56010 Pisa, Italy

[9]Centre d'Etudes Nucléaires de Saclay, F-91191 Gif-sur-Yvette Cedex, France

[a]On leave from Scuola Normale Superiore, Pisa and INFN, Perugia, Italy.

[b]Now at Fermilab, Batavia, ILL 60510, USA.

[c]Now at Université de Fribourg, CH-1700, Fribourg, Switzerland.

[d]Also at Dipartimento di Fisica dell'Università, Perugia, Italy.

[e]On leave from INFN, Pavia, Italy.

[f]Now at Dipartimento di Fisica dell' Università, Bologna, Italy.

[g]Now at Università di Milano, 20133 Milano, Italy.

[h]Now at Physics Department, Suny at Stony Brook, Stony Brook, NY 11794, USA.

[i]Now at SLAC, Stanford, CA 94305, USA.

[j]Cavendish Laboratory, University of Cambridge, Cambridge, U.K.

1 Introduction

In a previous publication [1] we reported results from a measurement of the direct production of photons with high transverse momentum (p_T) from $\bar{p}p$ collisions at an energy of $\sqrt{s} = 630$ GeV. These results were based on a data sample corresponding to a total integrated luminosity $\mathcal{L} = 310\,nb^{-1}$.

In a subsequent run during Autumn 1985 the total integrated luminosity was increased to $\mathcal{L} = 768\,nb^{-1}$. We present here a measurement of the inclusive cross-section of high p_T direct photons using the whole data sample. This cross-section is found to be in good agreement with a next-to-leading order QCD calculation [2].

We also study the structure of events containing a high-p_T photon, and we find that in most of the events the photon transverse momentum is balanced by that of a single jet. The features of the photon-jet events are compared with those of two-jet events and events containing a $W \to e\nu$ decay or a $Z \to e^+e^-$ decay.

Finally we observe a signal from production of direct photon pairs. The size of the signal is consistent with parton model expectations.

2 Apparatus

The UA2 detector [3] covers two distinct regions of polar angle: $40° < \Theta < 140°$ (the central region) and $20° < \Theta < 40°$, $140° < \Theta < 160°$ (the forward region). Both regions are covered by a central tracking chamber measuring the event vertex and the direction of charged tracks [4], and are also equipped with preshower detectors which in the present study function as active photon converters. In the central region the converter is a 1.5 radiation length thick tungsten cylinder. It is followed by a cylindrical multiwire chamber which, in association with the measured event vertex, determines the direction of a converted photon with a precision of 10 mr and resolves two adjacent conversion signals if they are separated by more than about 35 mr. In the forward region the preshower detector consists of a 1.4 radiation length lead-iron converter followed by a multi-tube proportional chamber [5]. Using the measured event vertex, this chamber is able to measure the direction of a converted photon with a precision of 2 mr.

An array of 480 calorimeter cells, each cell covering 15° in azimuth (ϕ) and about 0.2 units of pseudorapidity (η), measures the energy of electrons and photons. Each cell is segmented longitudinally to separate e/γ showers from hadron showers. In the central region, the calorimeter [6] has sufficient thickness (4.5 absorption lengths) to contain most of the energy in hadron showers. In the forward regions hadron showers are not fully contained. These regions are, however, equipped with magnetic spectrometers to measure the momenta of charged tracks.

3 Data reduction

The data were recorded with a trigger requiring a deposition of at least 10 GeV of transverse energy into a 2 x 2 cell matrix of the electromagnetic calorimeter in coincidence with a minimum-bias signal from small angle hodoscopes, which are used to suppress beam-halo background.

The copious production of high-p_T hadron jets [7] is responsible for most of the events in the data sample. Jets often contain high-p_T π^0 and η mesons which decay into two photons. Owing to the limited resolution of the detector the photon pairs may appear as single photons. However, direct photons are expected to be more isolated from other particles than high-p_T π^0's and η's, with the exception of the contribution to direct photon production from quark bremsstrahlung, which is expected to dominate at low p_T and to become less important at high p_T (at $p_T = 20$ GeV the bremsstrahlung contribution is expected to be about 35% of the inclusive direct photon production [8,9]).

We increase the fraction of direct photons in the data sample by selecting events containing isolated photon candidates, with the effect of suppressing the contribution from quark bremsstrahlung. Due to the different characteristics of the central and forward detectors, we use different selection criteria in the two regions.

In the central region, each event is required to have an energy cluster [10] well contained inside the central calorimeter. In order to avoid trigger inefficiencies, we require that the cluster has $p_T > 12$ GeV. Each cluster must satisfy the following isolation criteria:

- The cluster must have a small longitudinal and lateral size as expected

for isolated electrons or photons. The pattern of photomultiplier signals must be consistent with that observed for test-beam electrons [6].

- No charged track and at most one preshower signal may be found in a cone of $\sqrt{\Delta\phi^2 + \Delta\eta^2} < 0.25$ about the direction defined by the event vertex and the cluster centroid.

In the forward region, events are required to contain a calorimeter cell with $p_T > 12$ GeV. The additional requirement that at least 20% of the transverse energy deposited in the cell be balanced by other particles emitted elsewhere reduces the background from beam-halo particles. Other requirements on the cell energy deposition are:

- At most 2% of the cell energy may be deposited in the last 6 (out of 30) radiation lengths.
- Neighbour cells inside a cone of $\sqrt{\Delta\phi^2 + \Delta\eta^2} < 0.53$ must contain less than 2 GeV.
- No charged track may be found inside the cone.

There are 10220 events in the central region and 6107 events in the forward region with a photon candidate satisfying the selection criteria.

The efficiency of the selection criteria is measured by applying them on a sample of events containing a $W \to e\nu$ decay, for which the electron track is ignored and the electron energy deposition in the calorimeter is assumed to be due to a single photon. The efficiency for detecting a direct photon that has converted in the preshower detector is hereby found to be 0.59 ± 0.06 in the central region and by 0.69 ± 0.07 in the forward region. If the photon did not convert, the efficiency is $5\% \pm 2\%$ smaller in the central region because the shower penetrates deeper into the calorimeter and has a larger probability of being rejected by the cut on its longitudinal size. The estimate of the efficiency does not apply for photons produced by final state bremsstrahlung since such photons are not expected to be isolated like electrons from W decays.

4 Background calculations

The background caused by beam-halo particles and by single hadrons has been estimated [1] to be less than 2% of the photon candidate sample.

The only significant background is caused by multi-photons from π^0 and η decay. It is measured by considering the fraction of the events in which the photon candidate has begun showering in the preshower converter. We define a conversion by an associated signal in the central preshower detector exceeding 3 minimum ionising particle equivalents (mip) or a signal in the forward preshower detector exceeding 6 mip.

The conversion probability, ϵ_γ, of an incident single photon is calculated as a function of the photon energy using the EGS shower simulation program [11] and test-beam results. The same calculation correctly describes the response to test beam electrons in the central detector and to single photons from reconstructed π^0 decays in the forward detectors. We estimate the error on ϵ_γ to be less than ± 0.02.

The conversion probability, ϵ_π, for the multi-photon background from π^0 and η decay is calculated using ϵ_γ for each photon. The ratio of the number of η's to the number of π^0's is assumed to be 0.6 [12] . The multiplicity distribution of π^0's and η's in the background is estimated using the ISAJET Monte Carlo program [13]. The presence of multi-π^0 states in the background has only a small effect on the value of ϵ_π and it contributes ± 0.01 to the error on ϵ_π. The uncertainty in the two-photon resolution also introduces an error on ϵ_π at low p_T. However, this error is only ± 0.01 for $p_T > 15$ GeV. No such error is present in the forward regions, since the preshower isolation cut is not applied there.

The calculated values of ϵ_π and ϵ_γ are shown on Figure 1 as a function of p_T. The measured conversion fractions in the data, α, are bounded by the two curves. The distance of α to the curves determines the fractional multiphoton contamination $b(p_T)$:

$$b(p_T) = \frac{\alpha - \epsilon_\gamma}{\epsilon_\pi - \epsilon_\gamma}, \quad 0 < b(p_T) < 1 \tag{1}$$

It is seen in Figure 2 that the multi-photon background decreases with increasing p_T.

In the central region we expect $W \rightarrow e\nu$ decays to contribute about 10 events in the p_T interval between 30 and 40 GeV, as a result of inefficiencies in the electron track reconstruction. This contribution corresponds to 8% of the total number of photon candidate events found in the same p_T interval.

5 Inclusive cross-sections

The invariant inclusive cross-section for direct photon production is evaluated from:

$$E\frac{d\sigma}{d^3p} = \frac{N_\gamma(p_T)[1 - b(p_T)]}{p_T \Delta p_T \mathcal{L} \epsilon_c A(p_T)} \tag{2}$$

where $N_\gamma(p_T)$ is the number of photon candidates in a p_T bin of width Δp_T, $\mathcal{L}$ is the integrated luminosity corresponding to the data sample and ϵ_c is the efficiency of the selection criteria for detecting direct photon events. The geometrical acceptance, A(p_T), is estimated by Monte-Carlo simulation.

The results of the measurement are listed in Table 1 and are shown in Figures 3 and 4. Only p_T dependent errors are presented. These errors, which are mainly statistical, include, in the central region, a p_T dependent error on ϵ_π and a p_T dependent error on the geometrical acceptance, and in the forward region a p_T dependent error on ϵ_γ.

The p_T independent systematic uncertainty on the normalization of the cross-section is 20% . It includes, in the central region, contributions from a 1.6% uncertainty on the energy scale (10%), the efficiency of the selection criteria (10%), the observed conversion probability (8%), the calculation of ϵ_γ (8%), the calculation of ϵ_π (3%), the geometrical acceptance (5%) and the integrated luminosity (8%). In the forward region the uncertainty on the energy scale contributes 15% , the efficiency 10% and the integrated luminosity 8% . All these errors are added in quadrature.

As a check on the estimate of the systematic error, we have repeated the cross-section measurement in the central region using a different set of isolation criteria [14]. In this analysis only calorimeter and track information is used to select the photon candidates. The main requirement is that the energy detected by the calorimeter in a cone of size $\sqrt{\Delta\phi^2 + \Delta\eta^2} < 0.78$ around the photon candidate be less than 3.5 GeV. The selected sample contains more multi-photon background than the standard photon candi-

date sample. However, the corresponding cross-section agrees with that shown in Figure 3 within statistical errors. The measurement is also consistent, within systematic and statistical errors, with a similar measurement of the direct photon cross-section from the UA1 collaboration [15].

The results are compared with a next-to-leading order QCD calculation [2]. The calculation uses the Duke-Owens structure functions (set 1) [16] and the 'optimized' choice of Q^2 scales [17]. As the contribution from bremsstrahlung of the final state quarks is suppressed in the data, it must also be removed from the prediction. However, the exact strength of the suppression is not known to us. Therefore we compare the data with two curves calculated by excluding bremsstrahlung photons emitted at angles smaller than 30° (full curve) or 60° (dashed curve) with respect to the outgoing quark direction [18]. At large p_T, where the sensitivity of the calculation to the inclusion of bremsstrahlung and to the choice of scales is small, good agreement is observed between the measurement and the calculation. The same calculation agrees well with the direct photon cross-section measured for different beams and targets at lower collision energies [19,20,21,22,23].

In our p_T range the cross-section for inclusive production of direct photons is expected to be roughly proportional to the gluon structure function. However, at the large Q^2 values of relevance to this experiment, the gluon structure function is not very sensitive to the form determined in experiments at low Q^2 [9]. This is illustrated in Figure 5, where the data in the central region are compared with the results of a calculation which uses different forms of the gluon structure function, $xG(x)$, as obtained from fits to deep-inelastic muon-nucleon scattering data from the NA4 experiment [24] using different values of the QCD scale parameter Λ (the same value of Λ is used everywhere in the calculation). We note that the use of different Λ values in the fit to the NA4 data results in very different forms of the gluon distribution $G(x)$: for example, for $\Lambda = 100$ MeV one finds the approximate form $xG(x) \sim (1-x)^{10}$, while for $\Lambda = 250$ MeV the less steep form $(1-x)^{3.5}$ is obtained. Figure 5 shows that, above a p_T value of 20 GeV, our data are consistent with practically all values of Λ, and thus with all forms of $G(x)$ at low Q^2. The discrepancy between the data and the theoretical calculations at lower p_T values is most likely due to the effect of quark bremsstrahlung, which was not taken into account in these

calculations.

In Figure 6 we compare the inclusive cross-sections for direct photons and jets [7]. The ratio of the cross-sections integrated over the interval $p_T > 30$ GeV is measured to be:

$$\frac{\sigma_\gamma}{\sigma_{jet}} = (4.6 \pm 0.8(stat) \pm 2.1(sys))10^{-4} \quad (3)$$

where the largest contribution to the systematic error comes from the uncertainty in the normalization of the jet cross-section. The curves shown in Figure 6 represent leading order QCD calculations of direct photon production [8] and of jet production [25] using everywhere $Q^2 = {p_T}^2/4$, four quark flavours, and the Duke-Owens structure functions (set 1) [16]. By comparing the measured ratio with the ratio between the two curves, we obtain the following result for the strong coupling constant times the ratio of K-factors: $(K_{jet}/K_\gamma)\alpha_S = 0.14 \pm 0.07$. The result does not depend on the choice of Q^2.

In earlier publications [12,1] we presented a measurement of the inclusive π^0 cross-section at $|\eta| = 1.4$. We have repeated the measurement with increased statistics and using an improved algorithm for reconstructing the π^0 energy [14]. The results are listed in Table 1 and shown in Figure 7. The new results for the π^0 cross-section are consistent with, but typically 20% smaller than the previously published results.

6 The structure of direct photon events

In the parton model a high p_T direct photon is normally balanced at opposite azimuthal angle by a hadron jet.

We consider events with a photon candidate in the central calorimeter and define jets as additional energy clusters [10] in a fiducial region of the central calorimeter, i.e. within the pseudorapidity interval $|\eta| < 0.77$. The jets are ordered in decreasing transverse energies. In 40% of the photon candidate events with $p_T(\gamma) > 12$ GeV we find a jet, j_1, with $E_T(j_1) > 5$ GeV. Figure 8 shows that the distribution of jet azimuthal angles peaks sharply in the direction opposite to the photon. Figure 9 shows that the average ratio between the transverse energies carried by j_1 and the photon is about 0.9, independently of $p_T(\gamma)$. The frequency of observed jets agrees

roughly with that expected from a parton model simulation [8,16] of direct photon events taking into account the geometrical coverage and the jet energy resolution of the central calorimeter [6].

Adding together all the transverse energy detected in the apparatus, while excluding the transverse energy of the photon and j_1, we obtain a quantity, $\tilde{E}_T$, the transverse energy of the underlying event. The sum is extended over the interval $|\eta| < 1.7$, although the acceptance is not complete in the forward regions. Figure 9 shows that $< \tilde{E}_T >$ stays constant as a function of $p_T(\gamma)$.

These features are not specific of direct photon events. Similar results are found using a five times larger data sample in which the photon candidate is replaced by a multiphoton jet failing some of the isolation criteria. This sample is called the π sample for short since the energy cluster is generated by a narrow jet consisting mostly of π^0's and η's. Among the features discussed above, the only one distinguishing the π sample from the γ sample is a slightly larger average transverse energy in the underlying event as shown on Figure 9. We also show $< \tilde{E}_T >$ measured in events containing a $W \rightarrow e\nu$ decay (excluding here the electron energy). In these events $< \tilde{E}_T >$ is lower than in the $\gamma + jet$ events, but this difference is sensitive to possible systematic errors in the clustering algorithm which assigns energy depositions to j_1.

7 Photon-jet transverse momentum

The measurement of the transverse momentum of the $\gamma + j_1$ system, $\vec{p}_T(\gamma j)$, is affected by differences in the energy resolution and energy scale for photons and jets and by the presence of final state bremsstrahlung. However, the component of the total p_T perpendicular to the external bisector of the photon and jet directions, ${p_T}^\eta$ (see Figure 10), is less affected by intrumental biases. The *r.m.s.* value of this component is a factor of $\sqrt{2}$ smaller than the *r.m.s.* of $p_T(\gamma j)$, provided $\vec{p}_T(\gamma j)$ is isotropically distributed.

In Figure 10 the *r.m.s* of ${p_T}^\eta$ for $\gamma + jet$ systems is compared with that of two-jet systems [26]. In both cases the azimuthal separation of the two clusters is required to exceed 120°. When calculating ${p_T}^\eta$, we have merged nearby clusters into the two main ones in order to reduce the effect of final

state bremsstrahlung [26]. The data suggests a small difference between the $\gamma + jet$ systems and the two-jet systems. On the other hand, we observe no difference between the transverse momenta of $\gamma + jet$ systems and $\pi + jet$ systems, where the π belongs to the previously mentioned multi-photon background sample.

As in the case of two-jet production [26], we notice a slow increase of $p_T(\gamma j)$ with increasing γj mass: $r.m.s.({p_T}^\eta) = 5.3 \pm 0.1$ GeV for $M(\gamma j) \approx 30$ GeV and $r.m.s.({p_T}^\eta) = 6.6 \pm 0.5$ GeV for $M(\gamma j) \approx 80$ GeV.

We also compare the $\gamma + jet$ transverse momentum distribution with that of Z bosons. From the sample of 39 $Z \rightarrow e^+e^-$ decays [27] we find $r.m.s.({p_T}^\eta) = 6.4 \pm 0.8$ GeV.

A difference between the average values of ${p_T}^\eta$ and $\tilde{E}_T$ for $\gamma + jet$ systems and for other final states is expected from the different behaviour of quarks and gluons. The incoming gluons are expected to radiate more than incoming quarks. This would result in a larger transverse momentum of the scattered two-body system and a larger $\tilde{E}_T$ the larger the gluon contribution to the initial state [28]. The results discussed above, though consistent with this picture, are not precise enough to confirm it.

8 Photon-jet angular distribution

Nearly all of the subprocesses responsible for two-jet final states receive contributions from t-channel spin 1 exchange. For quark-gluon and gluon-gluon scattering, this is a consequence of the existence of a three-gluon vertex. Such diagrams do not contribute to direct photon production (in the Born approximation), and consequently the angular distribution of direct photons is expected to be less peaked in the forward direction than that of jets.

The distribution of scattering angles $d\sigma/d\cos\Theta^*$ for two-jet systems in the centre of mass of the colliding partons has been measured previously at the SPS Collider [26,29]. Using the same experimental definition of Θ^* [30], we have measured part of the angular distribution of $\gamma + jet$ systems and for $\pi + jet$ systems, where the π belongs to the previously mentioned sample of multi-photon jets. This latter sample is assumed to be representative of two-jet events as far as production properties are concerned. The events

are required to satisfy the following criteria:

- The vertex position must be less than 150mm from the apparatus centre.
- The largest p_T jet in the event must have $p_T(j) > 10$ GeV and $50^o < \Theta(j) < 130^o$, where the polar angle Θ is measured with respect to the apparatus centre.
- The azimuthal separation between the photon and the jet must exceed 140°.
- The $\gamma + jet$ transverse momentum must be smaller than $p_T(\gamma)/2$.
- No additional jet with $p_T > 5$ GeV and a direction closer than 60° to the photon direction is allowed.

Because of the limited aperture of the central calorimeter, the distribution can not be extended to values larger than $|\cos\Theta^*| \approx 0.5$ for the present data sample without using large acceptance corrections. However, the ratio between the $\gamma + jet$ and $\pi + jet$ angular distributions is independent of acceptance, since the measured velocity and mass distributions of the two systems are found to be almost identical. In Figure 11 the ratio is shown as a function of $\cos\Theta^*$ for the sample of $\gamma + jet$ and $\pi + jet$ systems with masses exceeding 30 GeV. The ratio is normalised to the ratio in the first bin of $\cos\Theta^*$. The values are corrected for the measured variation with $\cos\Theta^*$ of the multi-photon background contamination. It is checked that consistent results are obtained using subsamples of systems with different average velocities in the laboratory, and therefore different $\cos\Theta^*$ acceptance. It is also checked that the efficiency of the photon selection criteria, measured using the $W \rightarrow e\nu$ sample, is independent of polar angle. The result is compared with the ratio between the structure function weighted sums of lowest order QCD subprocesses leading to $\gamma + jet$ final states and two-jet final states. The result agrees well with the expected weaker forward peaking of photons as compared with jets.

9 Charged multiplicity

The main contribution to the direct photon production in our p_T range is expected to be QCD Compton scattering [8,9]. About 75% of the jets recoiling against a photon with $p_T \approx 16$ GeV are expected to be of quark origin. On the other hand, only 36% of jets from two-jet events in the same p_T range are expected to be of quark origin [31]. Since quarks are expected to fragment into a smaller number of particles than gluons [32], we expect a relatively smaller charged multiplicity associated with the recoil jet in the photon candidate sample than in two-jet events.

We study a sample of events containing a photon candidate and a jet with $p_T(j_1) > 10$ GeV in the central calorimeter which are separated by at least $\Delta\phi = 150°$. For comparison we use the π sample where a typical jet is expected to recoil against the trigger cluster. The average "photon"-jet mass in the two samples is 35 GeV. Figure 12 shows the track density as a function of the azimuthal distance from the trigger cluster. At all azimuthal angles the track density in the π sample is larger than that in the γ sample, which again is larger than the track density in events with a $W \rightarrow e\nu$ decay.

The difference in the total charged multiplicity in the hemisphere opposite the trigger is:

$$\bar{n}_{ch}\ (opposite\ \pi) - \bar{n}_{ch}\ (opposite\ \gamma) = 2.0 \pm 0.3 \qquad (4)$$

This number has been corrected for the $26 \pm 4\%$ π^0 background in the γ sample as well as for the $88 \pm 10\%$ track finding efficiency (resulting from the loss of tracks from the two-track resolution and the gain of spurious tracks from false combinations of track coordinates). The effect of applying the isolation criteria around the electron in $W \rightarrow e\nu$ events is a reduction of the multiplicity on the opposite side by 0.3 ± 0.4 particles. From this we estimate an additional systematic error on the difference of about 0.7 particles.

The difference in opposite side multiplicity is consistent with the expected difference between quark and gluon fragmentation using a QCD cascade model [33], but the data could also be explained by a different track density in the underlying event of the two samples.

10 Photon pairs

Two direct photons are expected to be produced at a rate of about 0.004 times the single photon rate [8] , and they have been observed in pp collisions at $\sqrt{s} = 63$ GeV [34] and in pC and πC collisions at $\sqrt{s} = 19.4$ GeV [35]. In our sample of $\bar{p}p$ collisions at 630 GeV, we find 4 events with two photon candidates, each having $p_T > 11$ GeV and $|\eta| < 0.83$. No other high-p_T particles are observed in these events.

Misidentified two-jet events and γ-jet events may contaminate the $\gamma\gamma$ sample. The probability of misidentification is given by the rejection factors of the γ selection criteria against multiphoton systems (r_π) and jets (r_j) :

$$\begin{aligned} r_\pi &= b\, n(\gamma)/n(\pi) = 0.056 \pm 0.006 \\ r_j &= r_\pi\, n(\pi\pi)/n(\pi j) = (2.2 \pm 0.4)10^{-4} \end{aligned}$$

where b is the background fraction shown in Figure 2 and n is the number of events containing clusters which are classified as either a photon candidate (γ), a multiphoton system (π) or a jet (j) with $p_T > 11$ GeV and $|\eta| < 0.83$. We get a consistent value for r_j by dividing the background rate by the extrapolation of the jet rate measured at very high p_T [7]. The background under the four $\gamma\gamma$ events is evaluated as $r_j\, n(\gamma j) = 0.74 \pm 0.12$ events. A similar result is reached using only r_π in the background calculation.

The efficiency of the selection criteria is taken as the square of the single photon efficiency ($\epsilon_c = 0.59 \pm 0.06$). The total cross-section is then:

$$\frac{d\sigma_{\gamma\gamma}}{d\eta_1 d\eta_2} = 4.8 \pm 2.5\ pb \quad (p_T{}^\gamma > 11\ GeV) \tag{5}$$

A leading order QCD calculation yields a cross-section: $\sigma_{\gamma\gamma}(L.O.) = 1.8\ pb$. In this calculation $\bar{q}q$ annihilation and gg annihilation through a quark loop [8] are folded with the Duke-Owens structure functions (set 1) [16] using $Q^2 = {p_T}^2$. A preliminary next-to-leading order calculation of two-photon production [18] yields approximately 4 pb, in good agreement with the measurement. We note that also in the case of single photon production, the lowest order calculation using $Q^2 = {p_T}^2$ results in a cross-section with about half the size of the full next-to-leading order prediction.

11 Conclusions

We have presented a study of direct photon production based on data from $\bar{p}p$ collisions at $\sqrt{s} = 630$ GeV. The inclusive cross-section is measured and found in good agreement with QCD theory.

Some features of the event structure in direct photon events have been studied. A jet balancing $\vec{p_T}(\gamma)$ is found with the frequency expected from the parton model. Together, the photon candidate and the jet dominate the transverse energy flow in the events. The rest of the particles detected by the apparatus carry an average sum of transverse energies which is independent of $p_T(\gamma)$. The r.m.s transverse momentum of $\gamma + jet$ systems is similar to that of two-jet systems and Z bosons. The angular distribution of two-jet systems is more peaked at small scattering angles than that of $\gamma + jet$ systems, in agreement with the QCD prediction. At all azimuthal angles, the track density in direct photon events is smaller than in events triggered by a multiphoton system and larger than in events triggered by a $W \rightarrow e\nu$ decay. A two-photon signal is observed, consistent with the cross-section expected from QCD theory.

Acknowledgements

The UA2 experiment would have been impossible without the successful operation of the CERN $\bar{p}p$ collider whose staff we gratefully acknowledge for their collective effort. We deeply thank the technical staff of the institutes collaborating in UA2 for their contributions to maintain and improve the detector. We are grateful to the UA4 collaboration for providing the signals from their small-angle scintillator arrays and to the UA5 collaboration for the loan of scintillator hodoscopes. We are indebted to P. Aurenche, R. Baier, M. Fontannaz and D. Schiff for providing the theoretical predictions subject to the experimental conditions for the present study.

Financial support from the Schweizerischer Nationalfonds zur Förderung der Wissenshaftlichen Forschung to the Bern group, from the Danish Natural Science Research Council to the Niels Bohr Institute group, from the Bundesministerium für Forschung und Technologie to the Heidelberg group, from the Institut National de Physique Nucléaire et de Physique de

Particules to the Orsay group, from the Istituto Nazionale di Fisica Nucleare to the Pavia, Perugia and Pisa groups and from Institut de Recherche Fondamentale (CEA) to the Saclay group are acknowledged.

References

[1] *UA2 coll.* J.A.Appel et al., Phys.Lett. 176B (1986) 239;

[2] P.Aurenche et al., Phys.Lett. 140B (1984) 87;

[3] *UA2 coll.* B.Mansoulié, Proc. 3rd Moriond Workshop on $\bar{p}p$ physics (1983) (Éditions Frontieres, Dreux, 1983) p.609;

[4] M.Dialinas et al., LAL Orsay preprint LAL-RT/83-14;

[5] K.Borer et al., Nucl.Instrum.Methods 227 (1984) 29;

[6] A.Beer et al., Nucl.Instrum.Methods 224 (1984) 360;

[7] *UA2 coll.* J.A.Appel et al., Phys.Lett. 160B (1985) 349;

[8] E.L.Berger et al., Nucl.Phys. B239 (1984) 52;

[9] J.F.Owens, Rev.Mod.Phys. 59 (1987) 485;

[10] *UA2 coll.* P.Bagnaia et al., Z.Phys. C20 (1983) 117;

[11] R.Ford and W.Nelson, SLAC-210 (1978);

[12] *UA2 coll.* M.Banner et al., Z.Phys. C27 (1985) 329;

[13] F.Paige and S.Protopopescu, BNL/81-31987;

[14] E.Lançon, Thesis, Université Paris 7, 1987;

[15] *UA1 coll.* C. Albajar et al., CERN-EP/88-45;

[16] D.W.Duke and J.F.Owens, Phys.ReV. D30 (1984) 49;

[17] P.Aurenche et al., Nucl.Phys. B286 (1987) 509;

[18] M.Fontannaz, private communication;

[19] *NA3 coll.* J.Badier et al., Z.Phys. C31 (1986) 341;

[20] *WA70 coll.* M.Bonesini et al., Z.Phys. C37 (1987) 535;

[21] *NA24 coll.* C.deMarzo et al., Phys.Rev. D36 (1987) 8;

[22] *UA6 coll.* A.Bernasconi et al., Phys.Lett. B206 (1988) 163;

[23] *R806 coll.* E.Anassontzis et al., Z.Phys. C13 (1982) 277;

[24] *BCDMS coll.* A.C.Benvenuti et al., Phys.Lett. B195 (1987) 97;

[25] B.L.Combridge et al., Phys.Lett. 70B (1977) 234;

[26] *UA2 coll.* P.Bagnaia et al., Phys.Lett. 144B (1984) 283;

[27] *UA2 coll.* R.Ansari et al., Phys.Lett. 194B (1987) 158;

[28] M.Greco, Z.Phys. C26 (1985) 567;

[29] *UA1 coll.* G.Arnison et al., Phys.Lett. 136B (1984) 294;

[30] J.C.Collins and D.E.Soper, Phys.Rev. D16 (1977) 2219;

[31] R.Horgan and M.Jacob, Nucl.Phys. B179 (1981) 441;

[32] J.B.Gaffney and A.H.Mueller, Nucl.Phys. B250 (1985) 109;

[33] B.R.Webber, Nucl.Phys. B238 (1984) 492;

[34] *AFS coll.* T.Åkesson et al., Z.Phys. C32 (1986) 491;

[35] *NA3 coll.* J.Badier et al., Phys.Lett 164B (1985) 184;

Inclusive direct photon and π^0 cross-sections $Ed\sigma/d^3p$ $(pb\,GeV^{-2})$ at $\sqrt{s} = 630$ GeV			
	$\bar{p}p \to \gamma + X$		$\bar{p}p \to \pi^0 + X$ [14]
p_T (GeV)	$\eta = 0$	$\eta = 1.4$	$\eta = 1.4$
13.0	30.8 ± 7.0	9.4 ± 3.2	154 ± 4
15.0	11.1 ± 1.3	6.4 ± 1.5	55.2 ± 1.7
17.0	4.9 ± 0.6	3.1 ± 0.8	21.7 ± 0.9
19.0	2.5 ± 0.3		10.6 ± 0.5
19.7		$9.9 \pm 3.0\ 10^{-1}$	
21.0	$12.8 \pm 1.9\ 10^{-1}$		$45.2 \pm 3.5\ 10^{-1}$
23.0	$7.4 \pm 1.1\ 10^{-1}$		$23.5 \pm 2.2\ 10^{-1}$
23.7		$3.0 \pm 1.2\ 10^{-1}$	
25.0	$4.0 \pm 0.9\ 10^{-1}$		$11.4 \pm 1.6\ 10^{-1}$
27.0	$2.0 \pm 0.5\ 10^{-1}$		$6.1 \pm 1.1\ 10^{-1}$
27.8		$1.9 \pm 0.7\ 10^{-1}$	
29.0	$16.6 \pm 4.0\ 10^{-2}$		
29.8			$28 \pm 6\ 10^{-2}$
31.8	$12.2 \pm 2.7\ 10^{-2}$		
33.0		$4.7 \pm 2.4\ 10^{-2}$	
34.7			$5.2 \pm 2.4\ 10^{-2}$
35.8	$7.3 \pm 1.8\ 10^{-2}$		
41.8	$16.2 \pm 4.2\ 10^{-3}$		
43.7		$5 \pm 4\ 10^{-3}$	$12 \pm 4\ 10^{-3}$
52.8	$19.4 \pm 9.3\ 10^{-4}$		
71.4	$4.3 \pm 2.1\ 10^{-4}$		

Table 1: The errors do not include the uncertainty of 20% on the normalisation. The last point at $\eta = 0$ is an average over the interval 60 GeV to 100 GeV in which 5 events are found.

Figure captions

Fig. 1 Conversion fractions for photon candidates in the central calorimeter (a) and in the forward calorimeter (b). The curves labeled ϵ_γ and ϵ_π are the conversion probabilities for single photons and multi-photon background, respectively.

Fig. 2 The fractional multi-photon background contamination in the sample of photon candidate events.

Fig. 3 The invariant differential cross-section for direct photon production in the central detector. The curves are explained in the text. See also Table 1.

Fig. 4 The invariant differential cross-section for direct photon production in the forward detector. The curves are explained in the text. See also Table 1.

Fig. 5 The invariant cross-section for direct photon production at $\eta = 0$ multiplied by ${p_T}^5$. The curves represent the QCD prediction for different gluon structure functions evaluated at $Q^2 = 2\ GeV^2$. The forms used for the gluon structure function are obtained from fits [18] to data from the NA4 experiment [24] using different values of the QCD scale parameter Λ.

Fig. 6 The differential cross-section for direct photon production and jet production at $\eta = 0$. The factor 1.45 is the ratio between the 630 GeV data and the 546 GeV data at $p_T \approx 35$ GeV [7]. The curves are the lowest order QCD predictions using the Duke-Owens structure function (set 1) and $Q^2 = {p_T}^2/4$.

Fig. 7 The invariant differential cross-section for π^0 production in the forward detector. See also Table 1.

Fig. 8 The azimuthal distribution of the largest E_T jet in events with a photon candidate in the central calorimeter. The jet must have $E_T > 5$ GeV and must be contained in the central calorimeter.

Fig.9 The upper part is the average ratio between the transverse energies of the largest E_T jet and the photon candidate as a function of $E_T(\gamma)$. The lower part is the average transverse energy in the underlying event, i.e. the total detected transverse energy excluding the trigger energy cluster and j_1, as a function of trigger transverse momentum.

Fig.10 The r.m.s. value of the component ${p_T}^{\eta}$ of the two-jet transverse momentum perpendicular to the bisector of the two jet axis. The dots show the quantity for two-jet systems [26] and the squares for $\gamma + jet$ systems as a function of the mass of the systems. The circle shows the corresponding quantity for $Z \rightarrow e^+e^-$ systems.

Fig.11 Ratio between the scattering angle distributions of $\gamma + jet$ systems and $\pi + jet$ systems, where the "π" is a multi-photon jet. The curve is the ratio between the subprocesses leading to $\gamma + jet$ final states and two-jet final states. The error on the first bin represents the normalisation error of the points relative to the curve.

Fig.12 The azimuthal distribution of charged tracks associated with a multiphoton jet (π), a photon candidate or a $W \rightarrow e\nu$ decay. The distributions have not been corrected for background and inefficiencies.

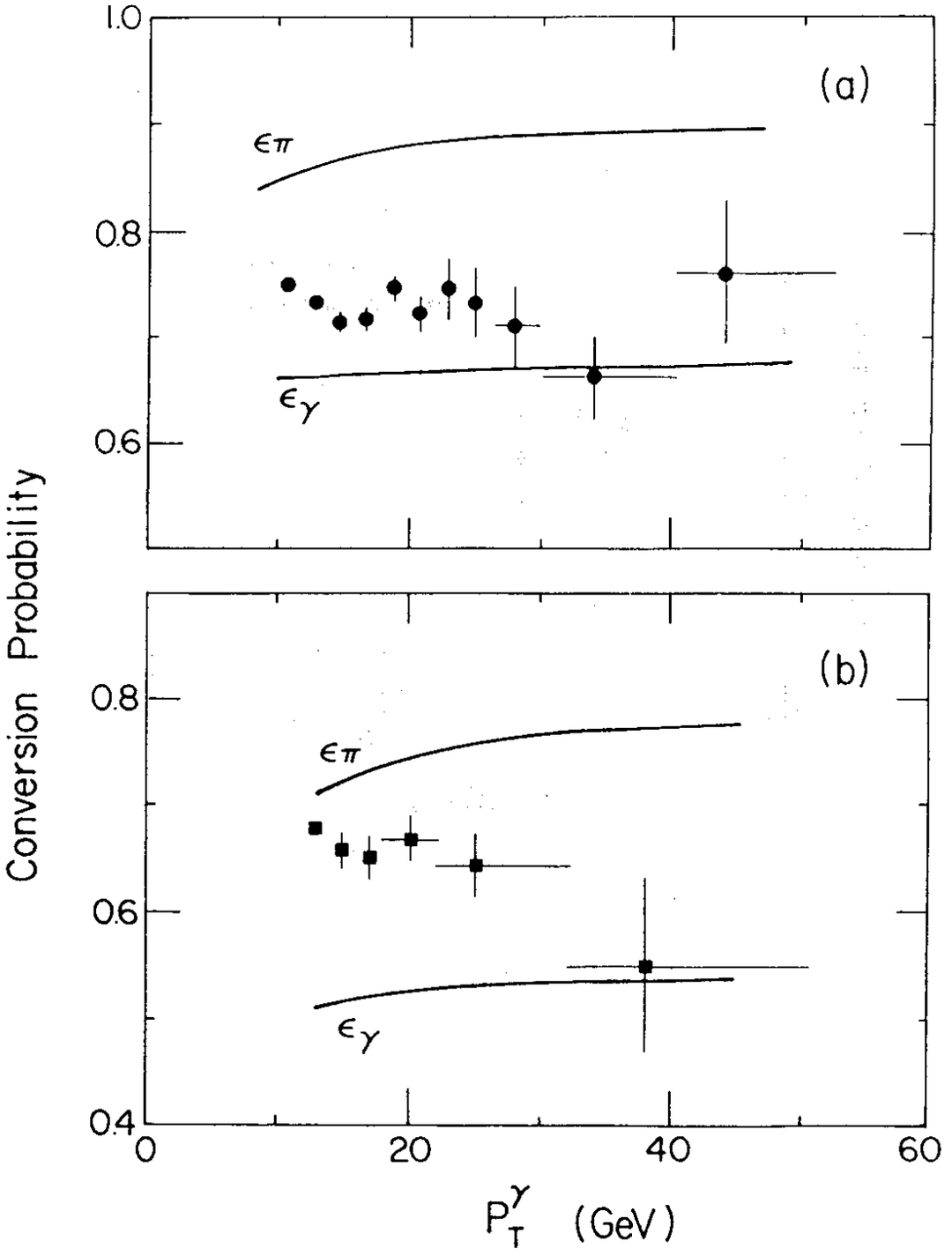
1.0
0.8
0.6
(a)
ϵ_π
ϵ_γ
0.8
0.6
0.4
(b)
ϵ_π
ϵ_γ
Conversion Probability
0
20
40
60
P_T^γ (GeV)

Figure 1

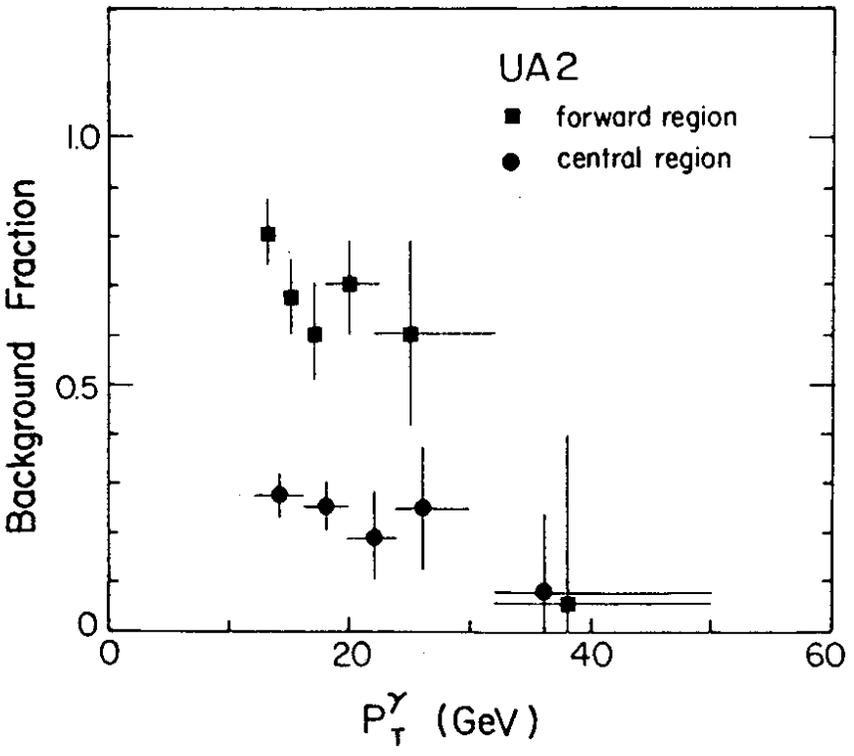
UA2
forward region
central region
Background Fraction
1.0
0.5
0
0
20
40
60
P_T^γ (GeV)

Figure 2

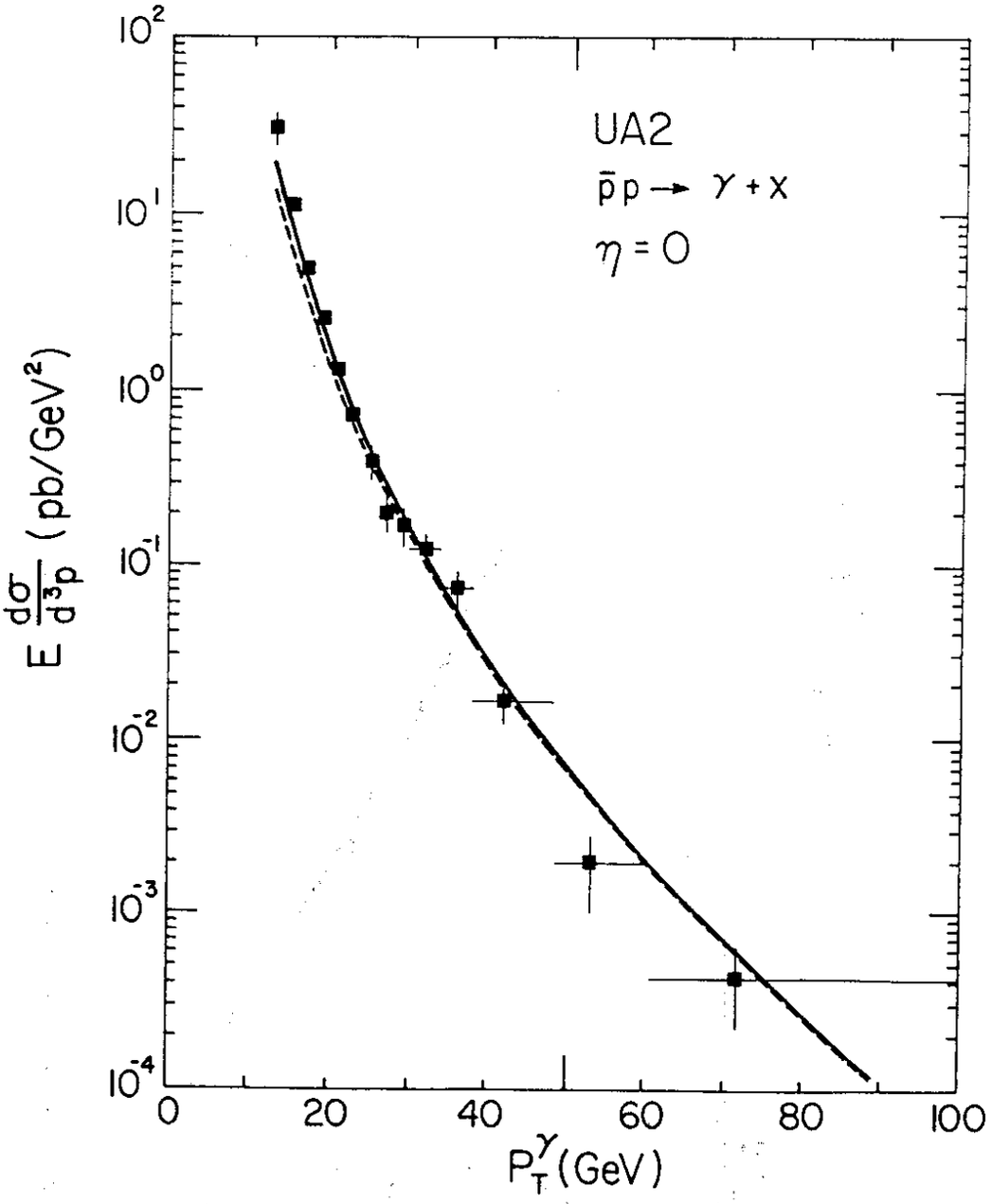
UA2
$\bar{p}p \rightarrow \gamma + X$
$\eta = 0$
$E\frac{d\sigma}{d^3p}$ (pb/GeV^2)
P_T^γ (GeV)
10^2
10^1
10^0
10^{-1}
10^{-2}
10^{-3}
10^{-4}
0
20
40
60
80
100

Figure 3

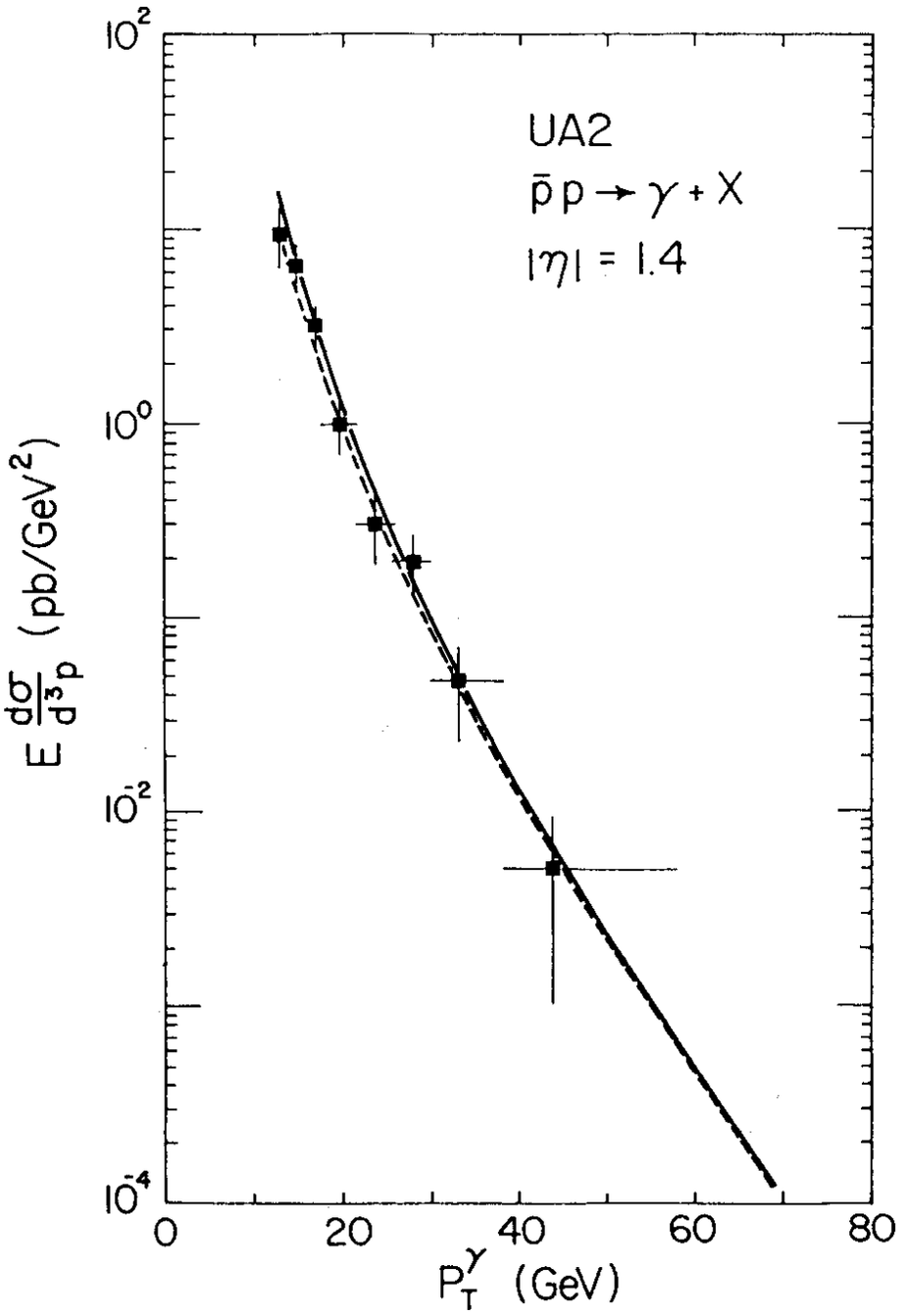
UA2
$\bar{p}p \rightarrow \gamma + X$
$|\eta| = 1.4$
$E\frac{d\sigma}{d^3p}$ (pb/GeV^2)
10^2
10^0
10^{-2}
10^{-4}
0
20
40
60
80
P_T^γ (GeV)

Figure 4

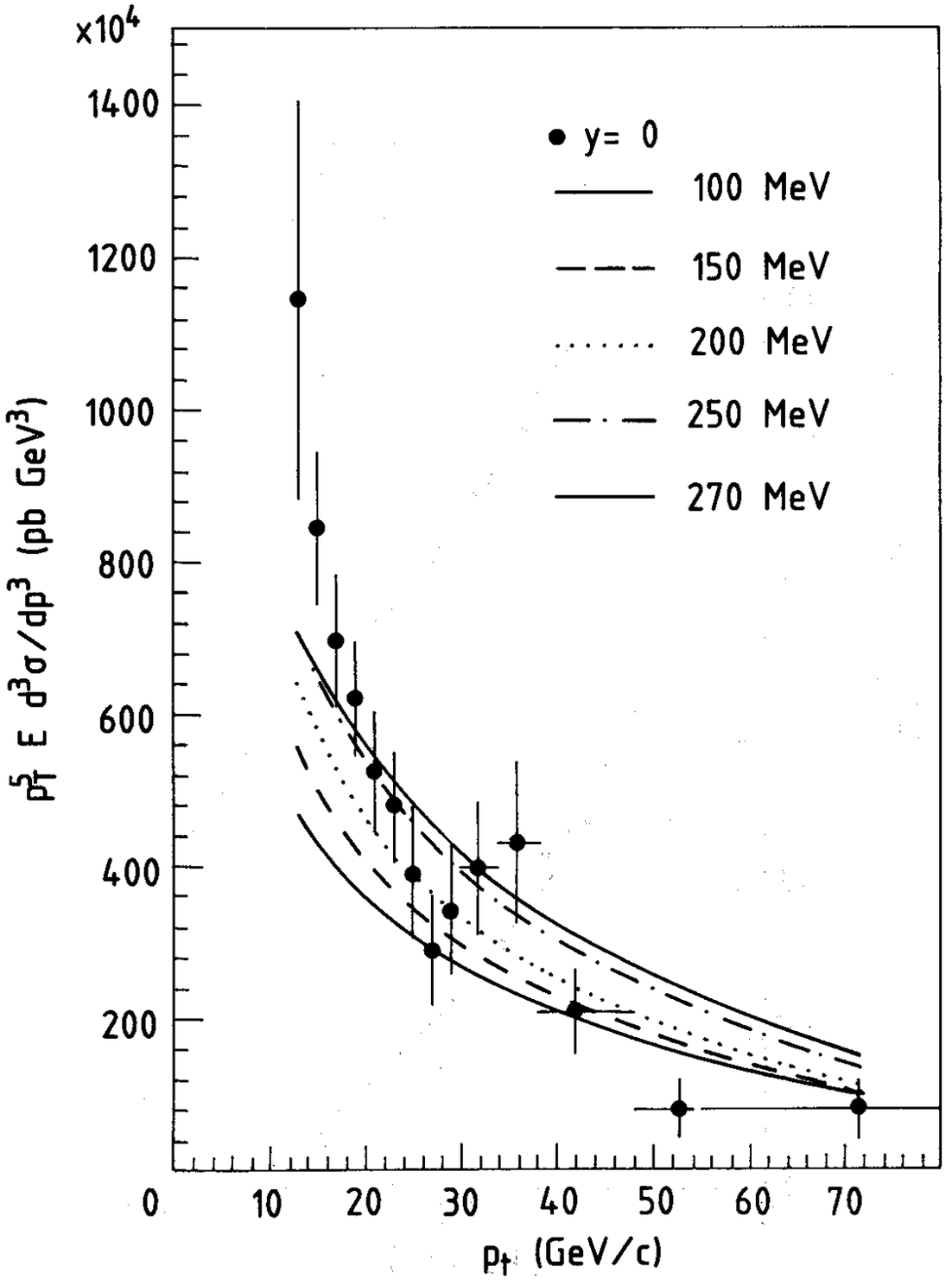
x10^4
1400
1200
1000
800
600
400
200
0
10
20
30
40
50
60
70
p_T (GeV/c)
p_T^5 E d^3σ/dp^3 (pb GeV^3)
y= 0
100 MeV
150 MeV
200 MeV
250 MeV
270 MeV

Figure 5

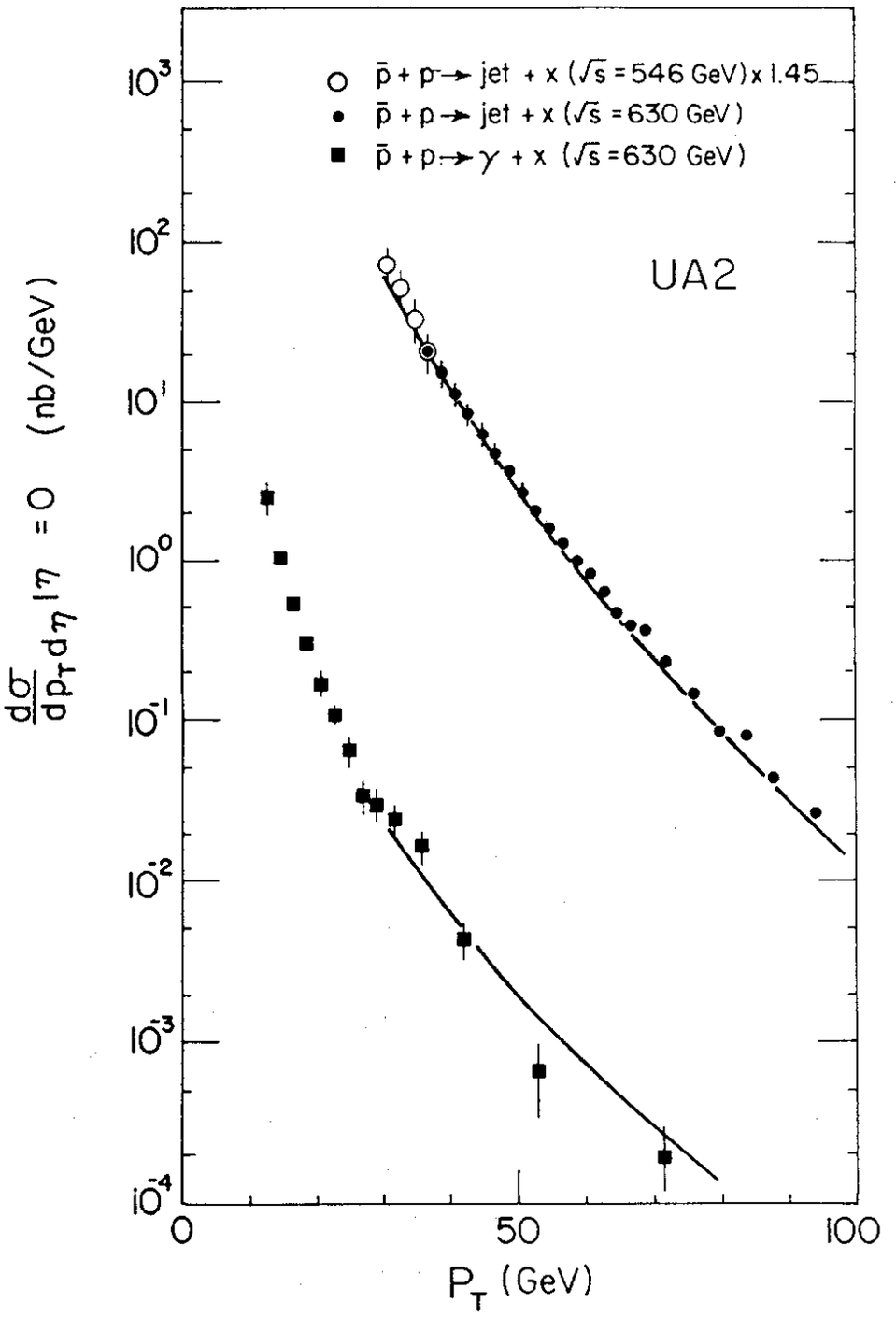
$\bar{p} + p \rightarrow$ jet + x ($\sqrt{s}$ = 546 GeV) x 1.45
$\bar{p} + p \rightarrow$ jet + x ($\sqrt{s}$ = 630 GeV)
$\bar{p} + p \rightarrow \gamma$ + x ($\sqrt{s}$ = 630 GeV)
UA2
$\frac{d\sigma}{dp_T d\eta}|_{\eta=0}$ (nb/GeV)
10^3
10^2
10^1
10^0
10^{-1}
10^{-2}
10^{-3}
10^{-4}
0
50
100
P_T (GeV)

Figure 6

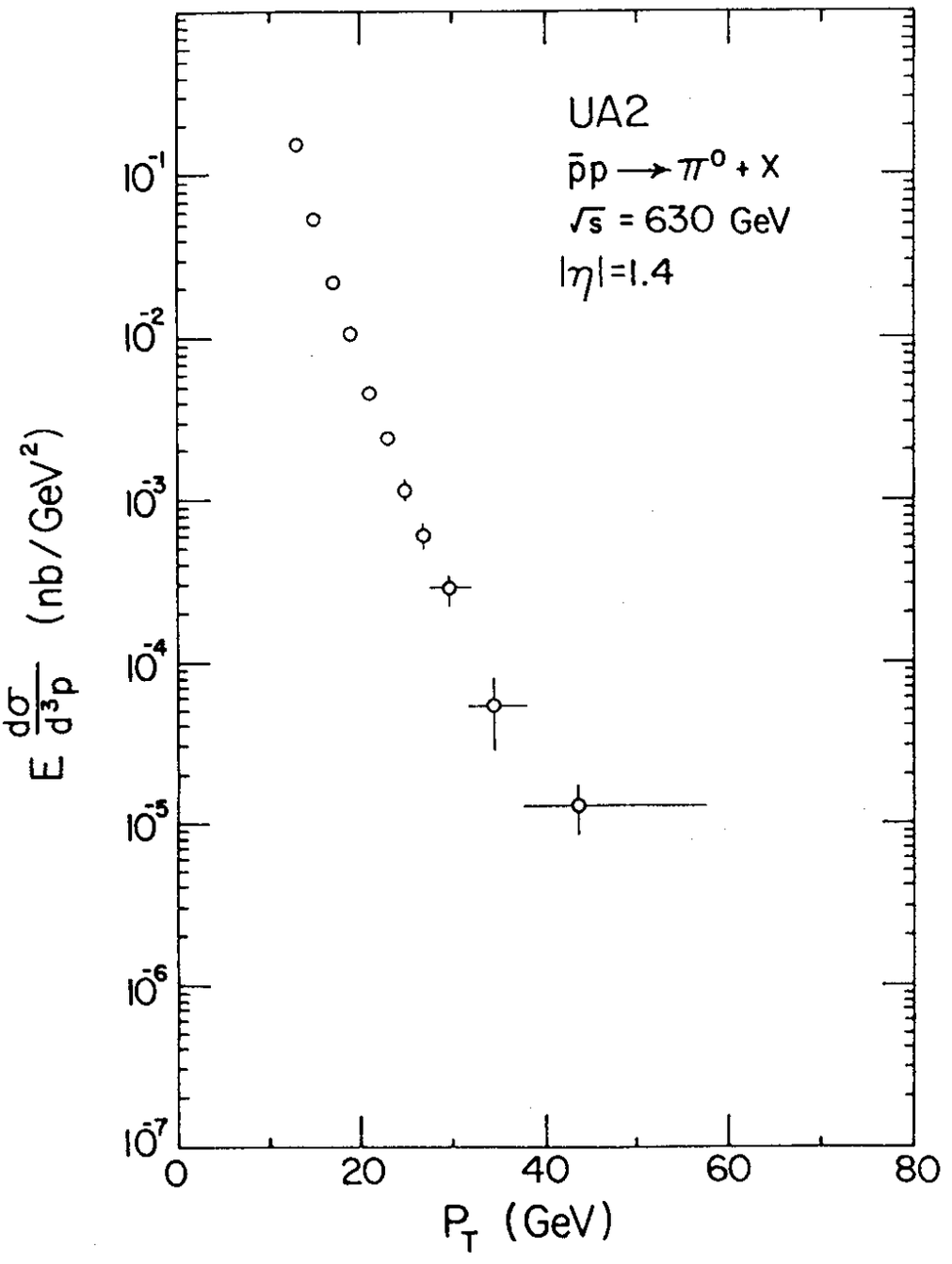
UA2
$\bar{p}p \rightarrow \pi^0 + X$
$\sqrt{s}$ = 630 GeV
$|\eta|$=1.4
$E\frac{d\sigma}{d^3p}$ (nb/GeV^2)
10^{-1}
10^{-2}
10^{-3}
10^{-4}
10^{-5}
10^{-6}
10^{-7}
0
20
40
60
80
P_T (GeV)

Figure 7

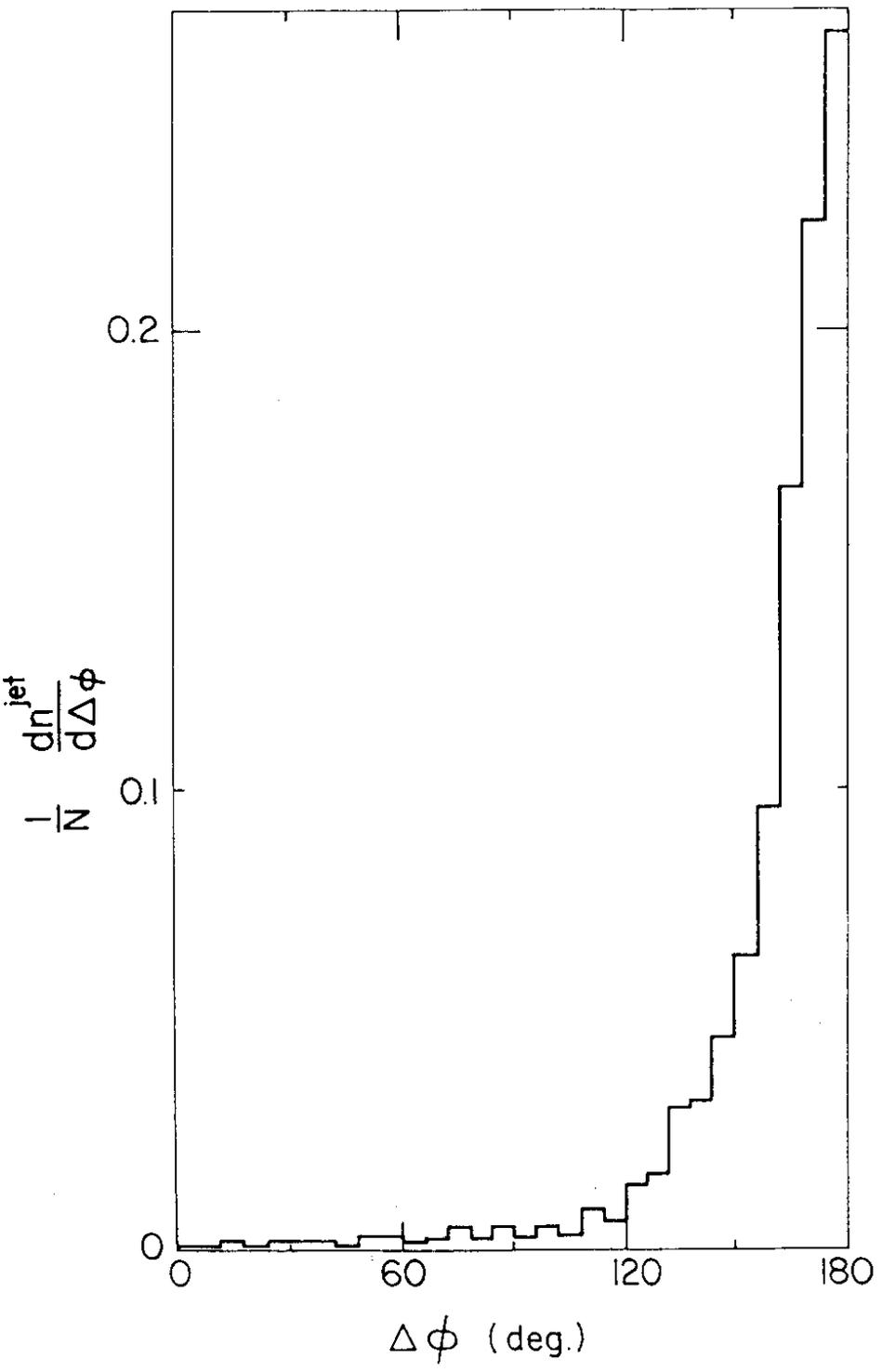

Figure 8

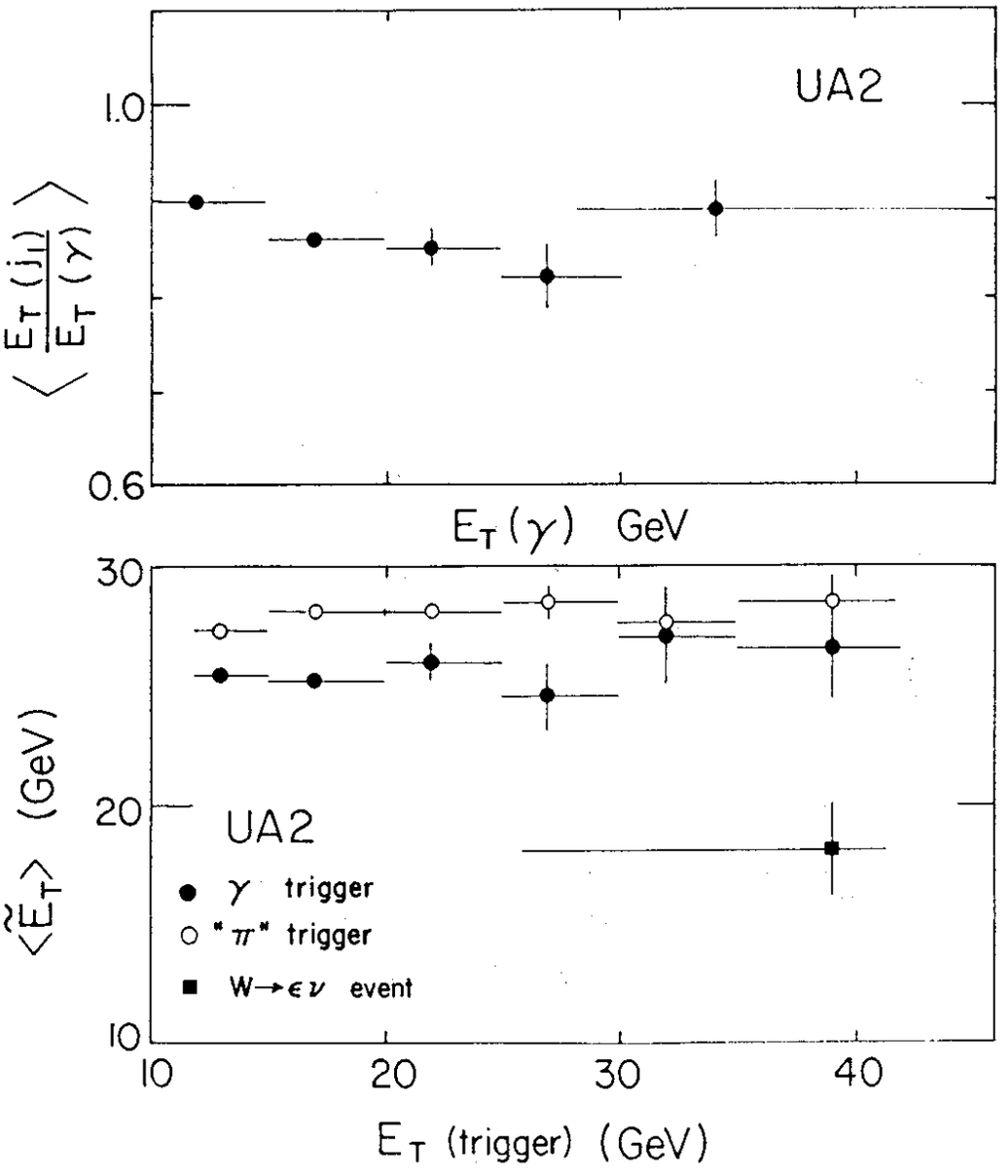
UA2
1.0
0.6
$\left\langle \frac{E_T(j_1)}{E_T(\gamma)} \right\rangle$
$E_T(\gamma)$ GeV
30
20
10
$\langle \tilde{E}_T \rangle$ (GeV)
UA2
● γ trigger
○ "π^0" trigger
■ $W \to e\nu$ event
10
20
30
40
E_T (trigger) (GeV)

Figure 9

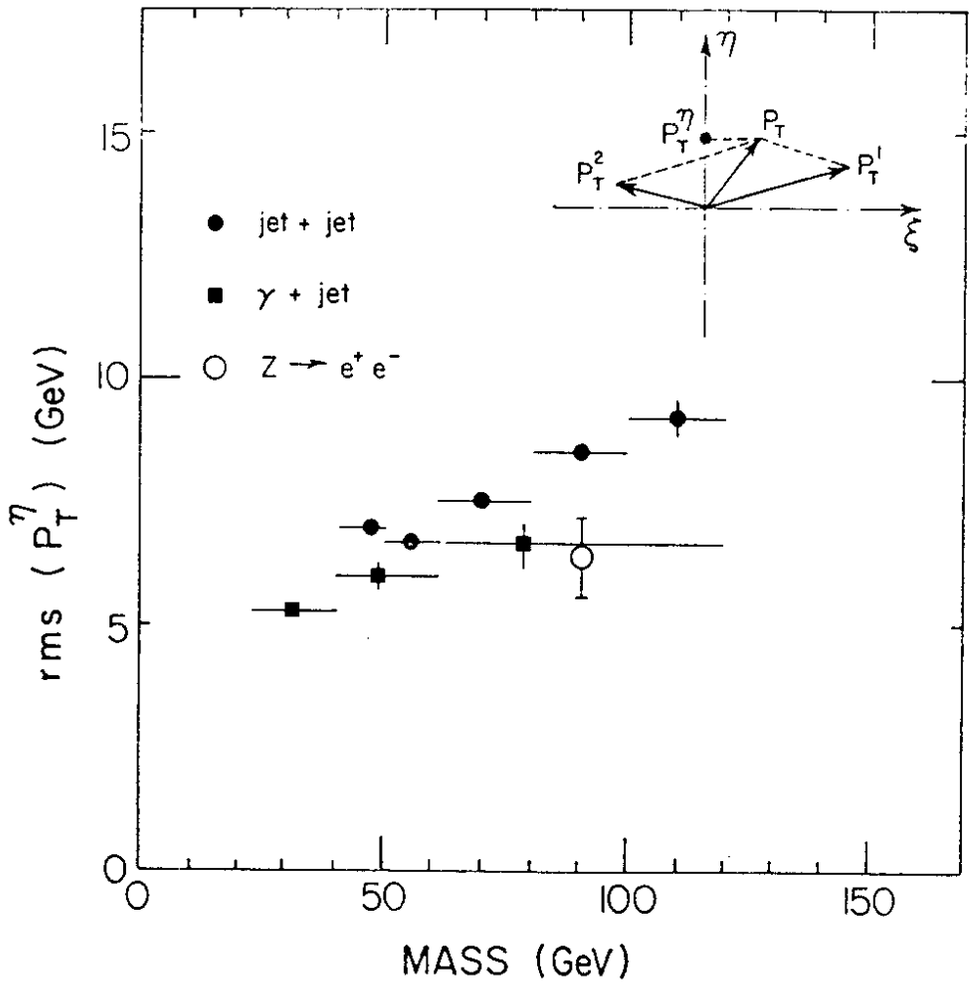
η
P_T^η
P_T
P_T^2
P_T^1
ξ
jet + jet
γ + jet
Z → e⁺ e⁻
rms (P_T^η) (GeV)
15
10
5
0
0
50
100
150
MASS (GeV)

Figure 10

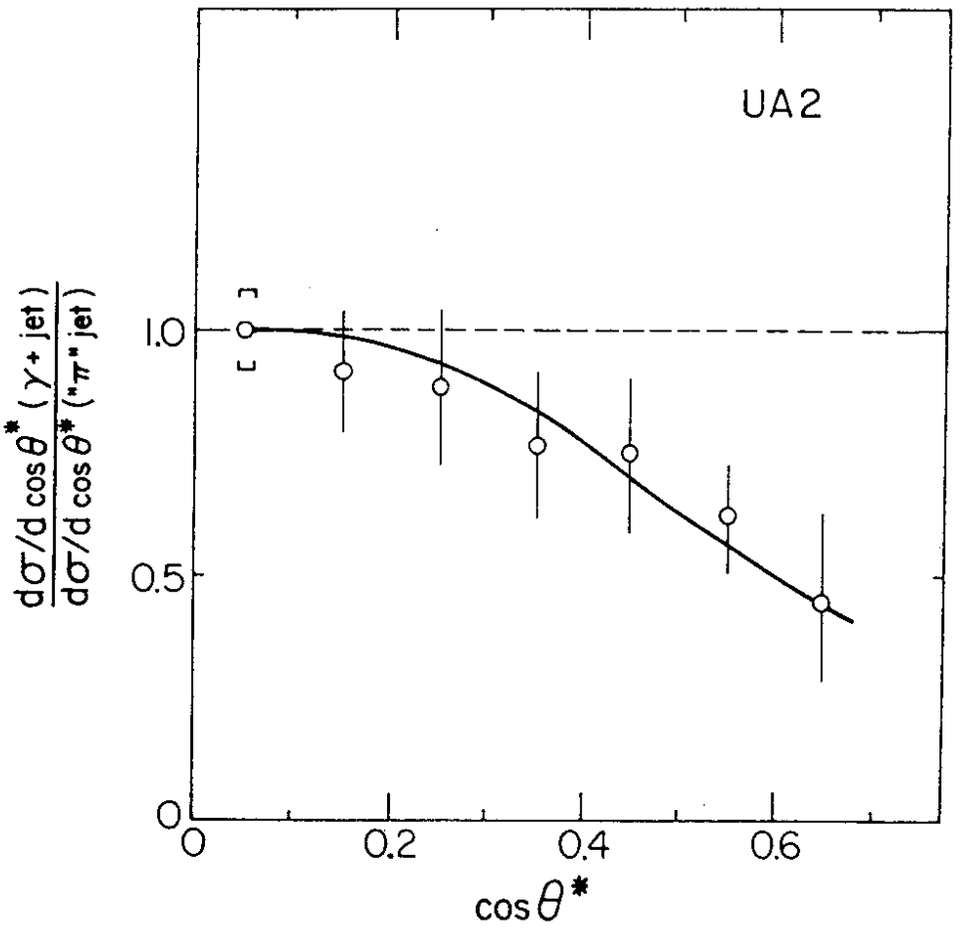
UA2
$\frac{d\sigma/d\cos\theta^*(\gamma+\text{jet})}{d\sigma/d\cos\theta^*(\text{"}\pi\text{"}\text{jet})}$
1.0
0.5
0
0
0.2
0.4
0.6
$\cos\theta^*$

Figure 11

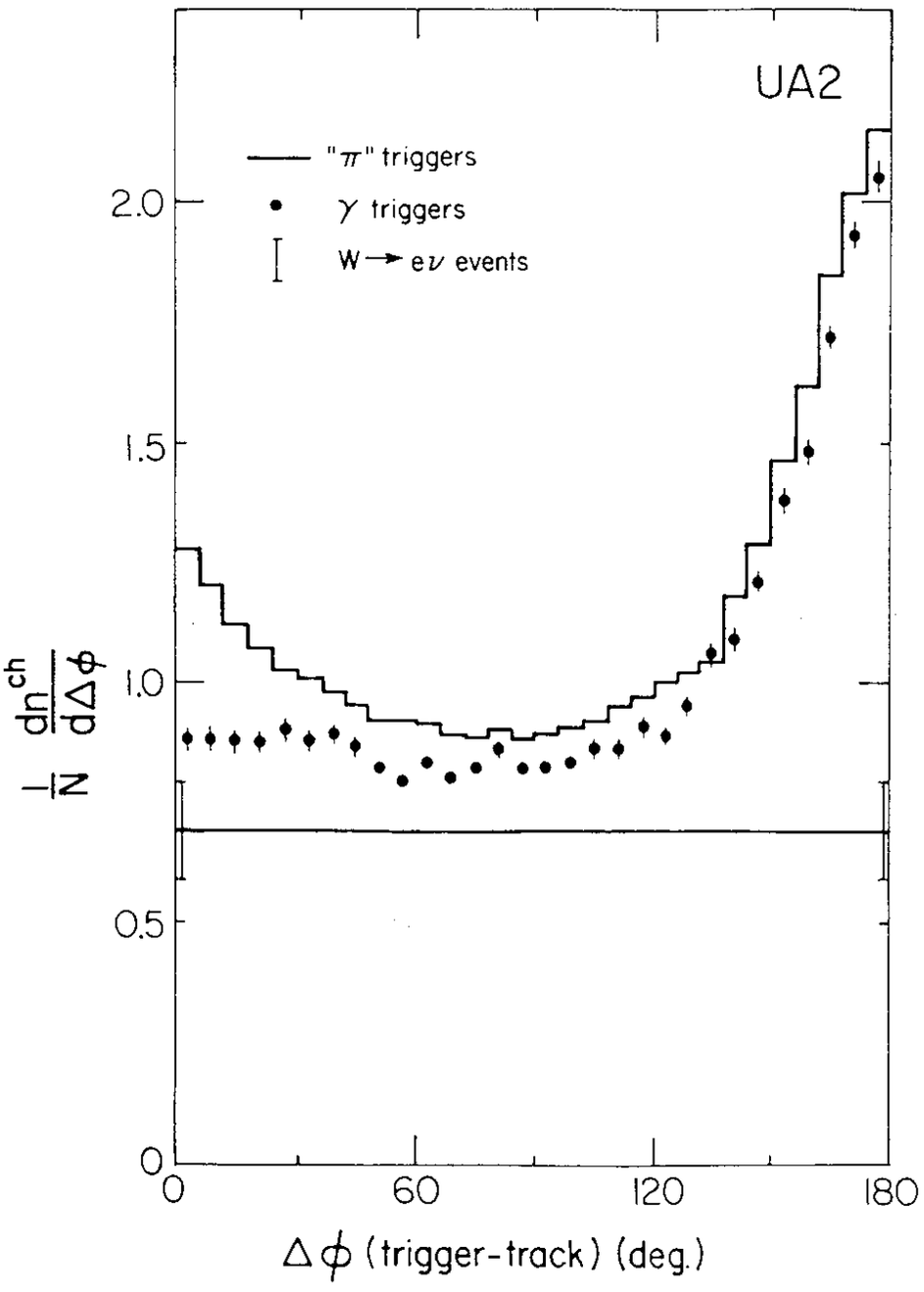
UA2
"π" triggers
γ triggers
W → eν events
2.0
1.5
1.0
0.5
0
0
60
120
180
$\frac{1}{N}\frac{dn^{ch}}{d\Delta\phi}$
Δφ (trigger-track) (deg.)

Figure 12